THE JOURNAL OF PHYSICAL CHEMISTRY C

Article

pubs.acs.org/JPCC

Rb^+ Adsorption at the Quartz(101)−Aqueous Interface: Comparison of Resonant Anomalous X-ray Reflectivity with ab Initio Calculations

Francesco Bellucci,[†] Sang Soo Lee,[†] James D. Kubicki,[‡] Andrei Bandura,[§] Zhan Zhang,[∥] David J. Wesolowski,[⊥] and Paul Fenter*,[†]

[†]Chemical Sciences and Engineering Division, Argonne National Laboratory, Argonne, Illinois 60439, United States

[‡]Department of Geosciences, The Pennsylvania State University, University Park, Pennsylvania 16802, United States

[§]Department of Quantum Chemistry, St. Petersburg State University, St. Petersburg, Russia

[∥]Advanced Photon Source, Argonne National Laboratory, Argonne, Illinois 60439, United States

[⊥]Chemical Sciences Division, Oak Ridge National Laboratory, Oak Ridge, Tennessee 37831, United States

Supporting Information

ABSTRACT: Adsorption of Rb^+ to the quartz(101)−aqueous interface at room temperature was studied with specular X-ray reflectivity, resonant anomalous X-ray reflectivity, and density functional theory. The interfacial water structures observed in deionized water and 10 mM RbCl solution at pH 9.8 were similar, having a first water layer at height of 1.7 ± 0.1 Å above the quartz surface and a second layer at 4.8 ± 0.1 Å and 3.9 ± 0.8 Å for the water and RbCl solutions, respectively. The adsorbed Rb^+ distribution is broad and consists of presumed inner-sphere (IS) and outer-sphere (OS) complexes at heights of 1.8 ± 0.1 and 6.4 ± 1.0 Å, respectively. Projector-augmented planewave density functional theory (DFT) calculations of potential configurations for neutral and negatively charged quartz(101) surfaces at pH 7 and 12, respectively, reveal a water structure in agreement with experimental results. These DFT calculations also show differences in adsorbed speciation of Rb^+ between these two conditions. At pH 7, the lowest energy structure shows that Rb^+ adsorbs dominantly as an IS complex, whereas at pH 12 IS and OS complexes have equivalent energies. The DFT results at pH 12 are generally consistent with the two site Rb distribution observed from the X-ray data at pH 9.8, albeit with some differences that are discussed. The surface charge estimated on the basis of the measured total Rb^+ coverage was −0.11 C/m^2, in good agreement with the range of the surface charge magnitudes reported in the literature.

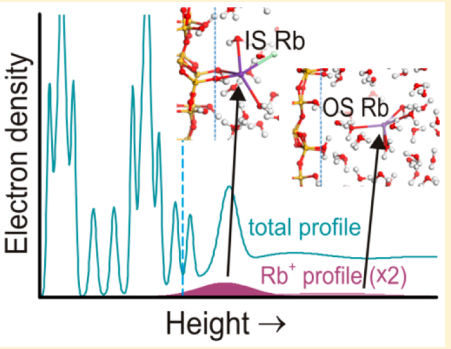

1. INTRODUCTION

Reactions at mineral−water interfaces affect a plethora of geochemical processes at Earth's surface.[1−3] Sorption at mineral surfaces effectively controls the mobility of natural and anthropogenic contaminants and toxic elements in natural waters, as well as mineral dissolution and precipitation, which control the bioavailability of inorganic nutrients, the chemical composition of groundwater,[1] and the evolution of porosity and permeability in geologic reservoirs.[4,5] Quartz is a major rock-forming mineral and accounts for about 20% of the crustal rocks exposed to weathering.[6] Although it is known to be less reactive than other silicate minerals,[7] quartz has a significant influence on the chemistry of numerous aqueous systems because of its abundance in nature.[8] In particular, the dissolution of quartz determines the concentration of silicic acid,[9] which controls the acidity of groundwater as well as pore water in many silica-rich soils.

Previous studies have focused on determining the surface charge of quartz and other SiO_2 polymorphs, including amorphous silica,[10,11] and its dependency on pH and dissolved electrolyte.[12−15] The surface charge determines the sorption capacity and ion selectivity. The surface charge in solution can be estimated on the basis of the difference between the solution pH and the point of zero charge (PZC). However, the large uncertainties in the reported silica/quartz PZC values (ranging from 2.1 to 3.8 pH units)[16] make accurate estimations of the surface charge difficult. For example, Bolt assumed a PZC of 3.5 and estimated the silica surface charge to be −0.13 ± 0.01 C/m^2 in a 0.01 M NaCl solution at pH 10, based on titration experiments.[10] Similarly, Ahmed assumed a PZC of ∼2.5 and estimated a surface charge of natural quartz from Brazil of −0.10 and −0.40 C/m^2 in 0.001 and 1 M KNO_3 solutions, respectively, at pH 10.[11] Dove and Craven directly measured the surface charge of silica through titration experiments using crushed quartz or colloidal silica particles in alkali- and alkaline earth-chloride solutions in the pH range 3−8.7 at 25 °C.[15] Their results suggest that at pH ∼8.5 the surface charge ranges from −0.10 to −0.15 C/m^2 for alkali metal solutions and from −0.15 to −0.20 C/m^2 for alkaline earth metal solutions (corresponding to 0.27−0.31 e^-/A_{UC} and 0.31−0.41 e^-/A_{UC}

Received: October 7, 2014
Revised: January 25, 2015

DOI: 10.1021/jp510139t
J. Phys. Chem. C XXXX, XXX, XXX−XXX

where A_{UC} = 33.8 Å ^{2} is the unit cell area of the quartz(101) surface). This technique is not applicable to SiO_2 powders at high pH (>9) where SiO_2 dissolution becomes significant.[15] The results also showed that, at constant ionic strength, the surface charge varies systematically with the solution electrolyte, and monovalent ions promote surface charge in a regular lyotropic series, while the alkaline earth cations follow a reverse lyotropic trend.[15,17]

The presence of electrolytes also affects quartz dissolution.[15,17−25] The effect of salt and pH on the dissolution rate was understood with its influence on step-motion[26] and models derived from classical crystal growth theory.[27] For example, cations enhance the dissolution rate with respect to that in pure water at near-neutral pH, in the order: $Mg^{2+} < Ca^{2+} \approx Li^+ \approx Na^+ \approx K^+ < Ba^{2+}$.[23] This enhancement is understood as a result of an increased dissolution reaction frequency (i.e., the prefactor in an Arrhenious relationship) rather than lowering of the reaction activation energy; this suggests that the dissolution rate may depend on a distinct structural relationship of the adsorbed ion with the surface atoms at the interface,[28] but the interaction of simple cations with the quartz surface remains poorly understood. Furthermore, Kubicki et al.[28] have suggested a new mechanism for quartz dissolution in aqueous electrolytes, involving intrasurface H-bond formation promoted by the close approach of dissolved cations to the surface as inner-sphere sorbed species.

X-ray reflectivity (XR) and resonant anomalous XR (RAXR) are powerful techniques that can be used to investigate the structure of the mineral−aqueous solution interface in situ and with atomic resolution.[29−32] In-situ X-ray measurements of the quartz−water interface have the potential to unravel the structural features that characterize the adsorption of ions and its relationship to the reactivity of the quartz surface. Previous XR studies at the quartz−deionized water (DIW) interfaces[33] demonstrated that it is possible to probe the molecular-scale structure of a natural quartz−water interface, and the results show good agreement with computational simulations.[34] These measurements have guided construction of atomic models for use in density functional theory (DFT) calculations. Energy minimizations using DFT and starting from observationally derived model structures have the capability of accurately reproducing XR and extended X-ray absorption fine structure (EXAFS) data.[35] In addition, when in agreement with experimental observations, the DFT-derived models provide more detailed information about the surface chemistry (e.g., protonation of surface oxygen atoms or H-bonding between the surface atoms and adsorbed water molecules) which is difficult to obtain from experimental measurements.

We present new high-resolution XR and RAXR results, complemented by density functional theory (DFT) calculations, applied to investigate the adsorption of Rb^+ ions at the natural quartz (101)−aqueous solution interface. Rb is chosen for these studies because it is chemically similar to the monovalent cations that are abundant in natural systems (e.g., Na^+, K^+) as well as radioactive contaminants such as $^{134}Cs^+$ and $^{137}Cs^+$. Direct observations of its adsorption structure through elemental specific X-ray based techniques thereby provide unique insights into the ion−quartz interactions that are inaccessible to any other approach. Thus, probing the interfacial structure of Rb ions at the quartz(101) surface provides an experimental test bed for validation of computational models[28] that can then be extended to a range of monovalent ions. The results reported here reveal the distribution of adsorbed Rb^+ at the surface, and offer insights into the quartz surface charge and the impact of cation adsorption on the interfacial structure.

2. MATERIALS AND METHODS

2.1. Sample Preparation. There are multiple experimental challenges in probing the interfacial structure of a natural quartz surface. First, there is potentially strong variability between samples (e.g., step morphology and terrace widths). Second, it is necessary to remove any accumulated foreign material so that the intrinsic behavior can be probed. While these challenges suggest that the use of synthetic quartz samples might be preferred, we find that polished synthetic surfaces are substantially rougher than the natural samples and typically have a poorly defined amorphous surface layer. This is attributed to mechanical polishing and can be expected to significantly alter the adsorption/dissolution behavior of the crystalline quartz surface. Consequently, we have chosen to study the behavior of natural growth surfaces that exhibit crystallographically controlled topographies.[33]

The RbCl solution was prepared by dissolving 300 ± 5 mg of high purity RbCl salt in 250 mL of DIW (with resistivity of 18.2 MΩ). The pH was adjusted to 9.80 ± 0.05 by adding a high purity 5 wt % RbOH solution while monitoring the pH with a Fisher Scientific Accumet Basic pH meter. The final solution had a Rb^+ concentration of 10 ± 0.5 mM.

Natural, optically clear quartz crystals from Herkimer County, New York ("Herkimer diamond") were used for this study. An optically flat slab of a (101) surface ("R", or main "pyramidal" face; ∼15 mm × 10 mm × 1 mm in size) was cut from the crystal using a low speed diamond saw. The sample was cleaned through sonication in acetone, methanol, and ∼10 wt % HNO_3 (in each for 15 min) to remove hydrophobic, amphiphilic, and hydrophilic contaminants, respectively. The sample was rinsed with DIW between baths. After this sequential cleaning procedure, the crystal was rinsed thoroughly with DIW and blow dried in a stream of purified N_2 for atomic force microscopy measurements (see section 2.2). Subsequently, the sample was annealed for 12 h at 400 °C in a vacuum furnace (furnace volume ∼ 2300 cm^3) under a ∼6 mL/min oxygen stream, to remove any additional organic contaminant that might be present. The sample was stored in DIW for 3 days prior to X-ray analysis.

2.2. Atomic Force Microscopy. The atomic force microscopy (AFM) images were collected in air using an Asylum Research MFP-3D AFM operated in AC ("tapping") mode to check the surface quality (e.g., step density and roughness). The probe was a silicon nitride (Si_3N_4) tip with nominal radius of 9 ± 2 nm and resonant frequency of ∼315 kHz, operated at a scanning rate of 1.0 Hz. Five 20 × 20 μm^2 areas were imaged to check for consistency in surface topography. Step height, distribution, and surface roughness were characterized using the Asylum Research AFM software (on WaveMetricsIGOR Pro platform).

2.3. X-ray Reflectivity and Resonant Anomalous X-ray Reflectivity. The sample was transferred to a thin film cell (Figure 1) for X-ray measurements using an 8 μm thick polyimide membrane (Kapton) as an X-ray window. The cell was drained by gravity until a thin (∼2 μm) uniform layer of solution was left above the sample to ensure minimal attenuation of X-ray beam in the liquid.

Specular XR and RAXR were measured at beamlines 6ID-B and 33ID-D at Advanced Photon Source (APS), Argonne

DOI: 10.1021/jp510139t
J. Phys. Chem. C XXXX, XXX, XXX−XXX

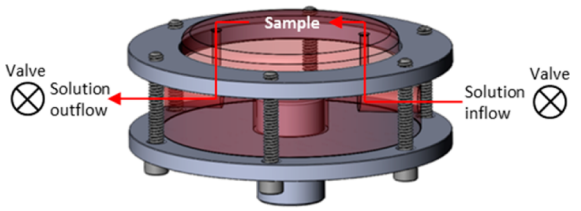

Figure 1. Schematic of the X-ray thin film cell used to collect the data presented in this study. The cell is sealed with a ~8 μm thick polyimide membrane, and the solution can be exchanged using a syringe. Typical sample dimensions: ~10 × 10 × 1 mm^3.

National Laboratory. All measurements were conducted in situ at room temperature. The beam size at the sample was 150 × 1000 μm^2 ($v \times h$) with a flux of ~5 × 10^{11} photons/s. The data were collected with a charge-coupled device (CCD) area detector. From each CCD image, the background was interpolated across the signal region using either a linear or polynomial regression line (chosen by the goodness of the fit to the background shape), and subtracted to isolate the reflectivity signal whose uncertainty was determined by counting statistics.[31] In spite of our extensive sample preparation, the quartz surfaces were found to be topographically heterogeneous. To address this issue, 2D maps of the reflectivity signal as a function of the beam footprint position were collected at a fixed scattering condition near the first midzone. Areas of the sample that showed high and uniform reflectivity, corresponding to areas with minimal roughness, were used to collect the data presented here. The stabilities of the interfacial systems were monitored by repeated measurements of XR and RAXR at selected q conditions. For the Rb data, the reversibility of Rb adsorption reactions was demonstrated by flushing the sample cell with 50 mL ultrapure DIW and observing that no Rb resonant signal was present after flushing (data not shown).

2.3.1. X-ray Reflectivity (XR). The XR signal, defined as the ratio of the reflected to incident X-ray flux, was measured at the quartz(101) − DIW and the quartz(101)−RbCl solution interfaces as a function of the momentum transfer (q), defined as $q = (2\pi/d)L$ where d = 3.3434 Å is the quartz(101) spacing and L is the Bragg index. The reflectivity $R(q)$ can be expressed as

$$R(q) = |B(q)|^2(4\pi r_e/qA_{UC})^2|F_{UC}F_{CTR} + F_{int} + F_w|^2 \quad (1)$$

where r_e = 2.818 × 10^{-5} Å is the classic electron radius, and A_{UC} = 33.8 Å^2 is the area of a unit cell along the (101) plane. F is a structure factor [for the substrate bulk unit cell (UC), interfacial region (int), or the fluid water (w)] defined as $F = \Sigma_j o_j f_j(q) \exp(iqz_j) \exp[-(qu_j)^2/2]$, where o is the occupancy, z is the height, u is the vibrational amplitude, and $f(q)$ is the atomic scattering factor of each atom, and the summation is over all atoms, j, within a specific substructure. $F_{CTR} = 1/(1 - \exp(-iqd/2))$ is the form factor for a semi-infinite crystal along the surface normal direction (Fenter, 2002). The prefactor, $|B(q)|^2 = (1-\beta)^2/[1+ \beta^2-2\beta\cos(qd)]$ where β ($0 \leq \beta \leq 1$) is the Robinson roughness factor,[29,31] accounts for the q-dependent reduction in the reflectivity signal associated with surface roughness. The XR data were collected at a photon energy of 18 keV and for q values between 0.1 and 5.8 Å^{-1}, corresponding to a range of Bragg index L from 0.05 to 3.09 reciprocal lattice units (rlu). The experimental resolution of the data (π/q_{max}) is ~0.55 Å for both data.[31]

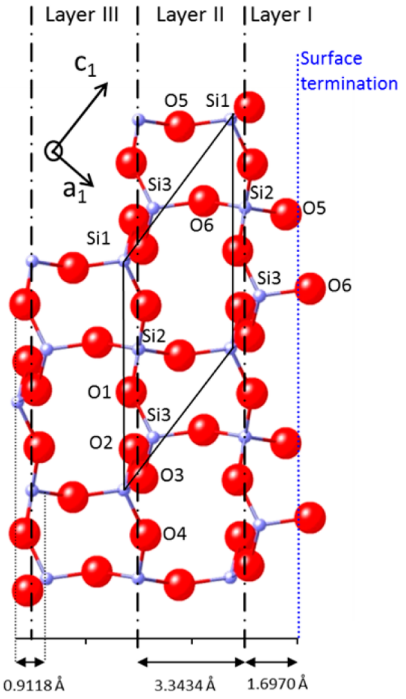

Figure 2. Section view of the quartz(101) structure projected along the a_2 axis. Thin black parallelogram shows a projection of one unit cell onto the (010) plane. Black dot-dashed lines indicate distinct layers and intersect the Si2 atoms. Redrawn after Schlegel et al. (2002),[33] with the origin for reference to atom heights chosen as the average height of the O5 and O6 terminal oxygens (blue dotted line).

The data were analyzed with a parametrized electron density model that consists of the following: (a) the unmodified subsurface crystal lattice; (b) an interfacial region that includes the relaxed quartz layers at the surface (the top three quartz unit cells for this study, Figure 2), the terminal oxygens (O5 and O6), and the surface-adsorbed species; and (c) the bulk solution above the surface. The origin for the reported atom heights (z = 0) is the average height of the *unrelaxed* O5 and O6 positions, and all relaxations are reported as the deviations from the bulk crystallographic positions. The vertical relaxation in the quartz surface was modeled by allowing Si1, Si2, Si3, and the terminal O5 and O6 to relax independently while restricting the vertical displacements of the remaining O atoms to be the average displacement of its two coordinated Si atoms. The occupancy factors of the Si atoms as well as their coordinated oxygen atoms in the top quartz unit-cell layer (Figure 2) were allowed to vary to simulate surface defects (e.g., atom vacancies) which can be present at the natural surfaces used in the current experiments. The electron density profile of the interfacial region is derived as the sum of the Gaussian distributions for each atomic layer, with parametrized occupancies, widths, and heights that are defined by the model fits. Various models for the interfacial water structure were explored (e.g., with 1−4 layers modeled by Gaussian functions followed by an error function profile extending beyond the last layer of structured water). The best fit model had two adsorbed water layers.

The model parameters were optimized through a nonlinear least-squares algorithm, and the goodness of fit was evaluated through the Pearson's chi-squared (χ^2) value defined as

DOI: 10.1021/jp510139t
J. Phys. Chem. C XXXX, XXX, XXX−XXX

$$\chi^2 = (1/N) \sum_i [(I_i - I_{calc})/\sigma_i]^2 \quad (2)$$

where N, I_i, I_{calc}, and σ_i are the number of data points, the measured and calculated intensity, and the statistical error in the measured reflectivity, respectively. The R-factor ($=[1/N]\Sigma_i|I_i - I_{calc}|/I_i$), reflecting the average fractional deviation between measured and calculated data, is also reported as another measure to quantify the fitting quality.

2.3.2. Resonant Anomalous X-ray Reflectivity (RAXR). The RAXR technique directly probes the element-specific electron density profile. The modulations of the energy-dependent X-ray reflectivity signal (referred to as RAXR spectra) from the quartz−water interface were measured as a function of the incident photon energy (E) near the Rb K-absorption edge at $E \sim 15.2$ keV for a series of fixed q values from 0.19 to 3.29 Å^{-1}, corresponding to Bragg indices L from 0.1 to 1.75 rlu, with a vertical resolution of ∼1 Å for the derived Rb distribution. The measured signal, $R(q_o, E)$, at each q_o value is controlled by the summation of the nonresonant structure factor (see section 2.3.1) and resonant structure factor (F_R) defined as

$$F_R(q_o, E) = \sum_j o_j[f_j'(E) + if_j''(E)] \exp(iq_o z_j) \exp(-q_o^2 \sigma_j^2/2) \quad (3)$$

where f_j' and f_j'' are the energy-dependent anomalous dispersion terms, related by Kramers−Kronig dispersion relationships,[36] and the resonant atom geometry is constrained by o_j, z_j, and σ_j (occupancy, height, and root-mean-square width of a Gaussian distribution for the jth atom, respectively). Several structural models were tested by varying the number of Gaussian peaks (from 1 to 3) to describe the interfacial density profile. The model using two Gaussians (referred to as the two-layer model hereafter) was chosen as the best-fit model on the basis of the goodness of fit (i.e., χ^2; see section 2.3.1) and the smallest sum of covariance among the fitting parameters.[37] We also attempted to fit the data using a diffuse ion-distribution model[38] to test the possible presence of a diffuse Rb profile at the interface. The result yields a Rb distribution that is very similar to that from the two-layer model but with a slightly larger χ^2 value (see Figure SI2 for details).

2.4. Density Functional Theory (DFT). Models of the α-quartz(101) surface were constructed in previous studies[28,39] and modified in this study to replace Na^+ with Rb^+ in order to investigate various Rb^+ sorption positions. The initial configurations used in this study (72 SiO_2, 77 H_2O, Rb^+ and Cl^- in a 14.6 × 9.82 × 39.2674 Å^3 cell with $\alpha = \beta = 90°$ and $\gamma = 109.6517°$) are the result of systematic construction from the bare (101) surface[39] as cleaved in the Surface Builder module of Materials Studio (Accelrys Inc., San Diego, CA), addition of H^+ and OH^- groups to the under-coordinated Si and O atoms (i.e., hydroxylation), and addition of H_2O molecules to form a monolayer at the surface (i.e., hydration). The vacuum gap between hydroxylated quartz slabs was then filled with 70 H_2O molecules that had been previously subjected to a 10 ps MD simulation at 298 K and 1 g/cm^3 using the universal force field to generate a configuration that would result in a well-behaved DFT-MD simulation.[28] In the earlier study,[28] Na^+ and Cl^- ions were placed in specific locations to manually search configuration space because extensive DFT-MD simulations are not practical. The Rb^+-containing simulations of this study were all derived from these previous configurations with modifications of the Rb^+ position to further explore potential configurations as suggested by experiment. Energy minimizations, then 8 to10 ps of DFT-MD simulations at 298 K with time step =0.5 fs were used to relax the SiO_2−Rb^+−Cl^-/OH^- models.[40] The (101) surface was modeled in a neutral state (i.e., fully hydroxylated and terminated with SiOH groups) and in a negatively charged state (i.e., one or two SiO^- groups = −0.05 and −0.10 C/m^2 respectively). The simulated solution contains one Rb^+ ion per 78 H_2O molecules, equivalent to a solution with 0.7 M Rb^+. The nominal pH of 12 corresponds to the system stoichiometry achieved by the replacement of one proton in the model by the Rb^+. In some models, to maintain pH neutrality, a Cl^- was introduced into the solution to charge-balance the extra Rb^+.

Projector-augmented wave method (PAW) calculations were performed with the Vienna ab initio simulation package VASP 5.2.[41] DFT methods included the following selection of parameters: Perdew−Burke−Ernzerhof[42] pseudopotentials, an energy cutoff of 500 eV, a single k-point centered on the Γ point of the Brillouin zone, a self-consistent field convergence criterion of 1×10^{-5} eV, and an energy minimization convergence of 0.02 eV/atom. The central layer of atoms in a five-layer thick quartz(101) surface slab was constrained in order to compare surface atom relaxations to the XR and RAXR measurements that determine surface atom positions relative to the bulk.[39] This methodology has previously reproduced the bulk structure of quartz to approximately 2% accuracy.[43] No dispersion force correction was employed, but ion−surface interactions should be dominated by electrostatics and polarization, and dispersion forces should be secondary in this system. Furthermore, it is not clear that dispersion force corrections in periodic DFT calculations will make the results more accurate with regard to experiment.[44]

3. RESULTS

3.1. Atomic Force Microscopy. Several quartz(101) surfaces were characterized using AFM prior to XR and RAXR measurements. These surfaces displayed a variety of step widths (typically 0.1−5 μm) and edge morphologies (from subparallel to sinuous and very sinuous). The step edges are mainly aligned along the [−2 −3 2] direction, as previously reported.[33] The sample selected for the X-ray measurements had regular (approximately parallel) steps that were ∼2 nm high and approximately 1 μm apart, and secondary steps 0.2−0.3 μm apart (Figure 3). The height for the smallest steps was 3.4 ± 0.5 Å, in agreement with the unit cell spacing normal to the (101) surface (3.3434 Å). Larger steps, from 11 to 25 Å are also present, corresponding to heights of approximately 3−8 unit cells. The surface had only negligible amounts of foreign particles.

3.2. X-ray Reflectivity (XR). The specular XR data for the quartz(101) surface in contact with DIW at pH 5.7 and the RbCl solution at pH 9.8 are shown in Figure 4 as a function of momentum transfer, q, along with the calculated reflectivity from the best-fit models. The two XR data sets are similar; however, visible differences emerge at q values corresponding to the anti-Bragg conditions where the interfacial sensitivity is maximized. The present results are also similar to those obtained on the annealed natural quartz(101) surfaces in water by Schlegel et al.,[33] except small intensity differences at q values of ∼1, and ∼4.2 Å^{-1}. The present data were measured with a finer q spacing between data points, higher precisions, and with

DOI: 10.1021/jp510139t
J. Phys. Chem. C XXXX, XXX, XXX−XXX

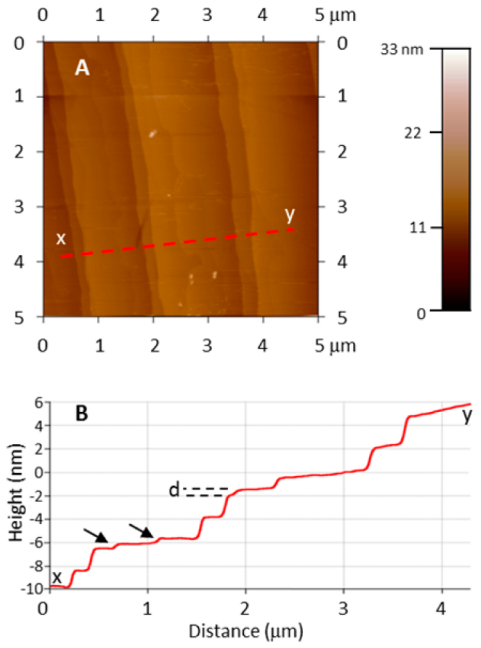

Figure 3. (A) 5 × 5 μm^2 micrograph of the cleaned quartz(101) surface by atomic force microscopy showing ∼1 μm wide major terraces alternating with narrower, ∼0.3 μm wide minor terraces. (B) Cross-section, x−y, indicated by the red dashed line in part A. The height of the smallest step, d ∼ 3.34 Å, corresponds to the height of one unit cell, with the black arrows highlighting the location of additional monatomic steps. This surface profile corresponds to a local miscut of 0.2°.

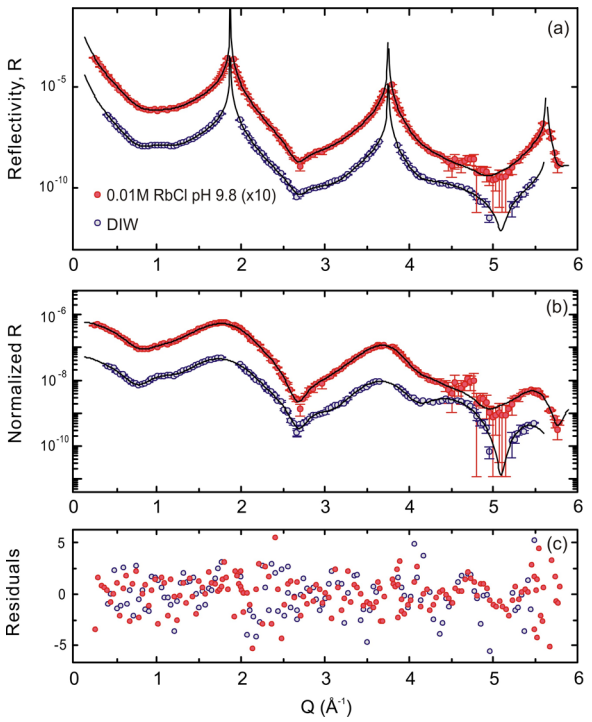

Figure 4. (a) Specular XR signal, $R(Q)$, of quartz(101) in contact with DIW (empty blue circles), and RbCl solution 0.01 M at pH 9.8 (full red circles), as a function of vertical momentum transfer, Q. (b) The same data after normalization by the generic CTR shape for quartz(101), $nR(Q) = R(Q)[Q^2\sin^2(Qc/2)]$; (c) residuals, $(R_i - R_{calc})/\sigma_i$, for the best-fit model. The reflectivity from the best fit models are represented by black lines. The RbCl data in parts a and b are scaled vertically (×10) for clarity.

a larger data range (corresponding to a higher vertical spatial resolution).

The best-fits obtained by comparison to parametrized electron density profiles (Table 1) reproduce the features in the XR data for both systems. The solution structure at the quartz−DIW interface was best fit with two Gaussian layers followed by a featureless water profile[31] to yield the χ^2 value of 3.82 and the R-factor of 0.097. The derived profile for the quartz−RbCl interface data has quality of fits of χ^2 = 2.23 and R-factor = 0.11.

The best-fit results for both data sets show similar relaxation parameters for the atoms near the quartz(101) surface. The absolute magnitudes of the relaxation of the individual Si atoms are relatively small (generally ≤0.1 Å) and tend to decrease into the bulk (Figure 5). Unlike these, the terminal oxygens O5 and O6 show relatively large negative displacements. We have explored whether the observed displacements of O5 and O6 terminal hydroxyl oxygens from the crystallographic locations might be attributed to the detachment of O5 and O6 from the surface by using structural models in which one or both of these surface oxygen atoms were removed. The results invariably provided poorer data fit quality, indicating that the observed large distortions of the (101) surface is due to the movements of the O atoms rather than breaking of Si−O bonds.

The best fit model suggests that Si3 vacancies are present in the topmost quartz layer (∼23−35% of the total), as well as a small amount of Si2 vacancies (∼7%) in the case of the quartz−RbCl interface model. The derived electron density profiles (Figure 6) for the two systems are similar to each other; however small differences are present due to the contribution to the total electron density profile from the Rb distribution at the interface. For both systems, the best-fit models show a relatively sharp electron density layer located at 1.7 ± 0.01 Å above the surface (defined as the average height of the two terminal oxygens O5 and O6 in the *unrelaxed* bulk-like structure) and a second broader layer at 4.8 ± 0.1 Å or 3.9 ± 0.8 Å for DIW and RbCl, respectively. When the O5 and O6 negative relaxations (which average −0.21 Å) are taken into account, the effective water layer heights above the surface become 1.9 ± 0.01 and 5.0 ± 0.1 or 4.1 ± 0.8 Å for DIW and RbCl, respectively.

3.3. Resonant Anomalous X-ray Reflectivity (RAXR). A total of 11 RAXR spectra (with 0.19 $Å^{-1} \leq Q \leq$ 3.29 $Å^{-1}$; Figure 7) were analyzed with a model-independent analysis (see Figure SI1) and by comparison to parametrized electron density profiles for the Rb ion distribution. The model-independent analyses[32] reveal amplitude and phase variations that cannot be described by a single adsorbed species but instead are indicative of profiles with two distinct ion heights near ∼1.6 and >4 Å (Figure SI1). The optimized model (with quality of fits of χ^2 = 1.11 and R-factor =0.014) has Rb heights of 1.6 ± 0.1 and 6.2 ± 1.0 Å (Table 1 and Figure 6, inset). When the O5 and O6 negative relaxations (which average −0.21 Å) are taken into account, the heights of Rb above the *surface* become 1.8 ± 0.1 and 6.4 ± 1.0 Å, respectively. In the discussion (section 4), we will use these values to compare with the results of the DFT calculations. The uncertainty of the height of the second Rb layer is somewhat large because of its smaller occupancy and the partial overlap with the first Rb layer. The occupancies of these two layers are 0.16 ± 0.02 and

DOI: 10.1021/jp510139t
J. Phys. Chem. C XXXX, XXX, XXX−XXX

Table 1. Structural Parameters Derived from the Best-Fit Models for Quartz(101) in Contact with DIW and 0.01M RbCl Solution at pH 10, Respectively[a]

		DIW		Rb		
	Parameter	value	σ	value	σ	
CTR results	β	0.00	0.00	0.21	0.02	Adsorbed layers
solution	Z2	4.8	0.07	3.9	0.78	
	occ2	8.83	0.65	12.62	4.82	
	Z1	1.7	0.01	1.7	0.01	
	occ1	3.98	0.22	2.30	0.12	
surface →	δO6	-0.25	0.020	-0.29	0.018	
	δO5	-0.15	0.036	-0.13	0.029	
	δSi3	0.17	0.018	0.04	0.021	
	occ Si3	0.65	0.05	0.77	0.03	
	δSi2	0.07	0.008	0.08	0.001	I
	occ Si2	1.00	0.01	0.93	0.02	
	δSi1	-0.04	0.009	-0.02	0.001	Quartz layers
	occ Si1	1.00	0.01	1.00	0.01	
	δSi3	0.03	0.009	0.03	0.003	
	δSi2	0.05	0.007	0.01	0.003	II
	δSi1	-0.04	0.006	-0.01	0.005	
	δSi3	-0.01	0.004	0.00	0.003	
	δSi2	0.00	0.003	0.01	0.002	III
bulk	δSi1	-0.02	0.004	-0.02	0.002	
	χ^2	3.82		2.23		
	R-factor	0.097		0.11		
	n param	20		21		
RAXR results	Z2			6.21	1.00	
	occ2			0.07	0.01	
	Z1			1.58	0.10	
	occ1			0.16	0.02	
	χ^2			1.11		
	R-factor			0.014		

[a] ***β***: surface roughness as defined in Robinson.[29] **Z**(*j*), **occ**(*j*): height above the surface and occupancy of the *j*th layer; (*j*) = 1 or 2. **δO5−6**: vertical relaxation of O5 and O6 terminal oxygen atoms. **δSi**(#): vertical relaxations of the Si (# = 1, 2, 3) atoms in the I, II, and III layer from the surface toward the bulk (refer also to Figure 2). **Occ Si**(#): fractional occupancy of Si (# = 1, 2, 3) in the topmost layer of the quartz surface. This parameter accounts for Si vacancies in the quartz layer in direct contact with the solution. **n param**: number of parameters used to fit the data. All relaxations are calculated from the respective atom position in the bulk-like structure, all distances are calculated from the crystal termination (average of O5 and O6 positions in the *unrelaxed*, bulk-like structure) and shown in units of Å. Occupancies of adsorbed layers are normalized to the scattering amplitude of the oxygen atom in a water molecule (shown in units of oxygen equivalents) while that of Si is shown as simple occupancies.

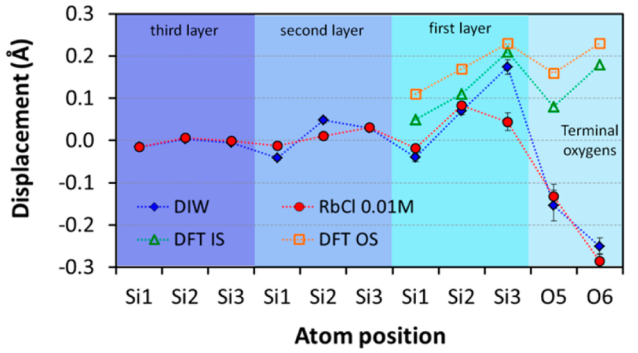

Figure 5. Vertical relaxations of the three topmost layers of the quartz(101) surface (~10 Å) in contact with DIW (blue diamonds) and RbCl 0.01 M pH 9.8 solution (red circles). The bridging oxygens (O1−O4) are assumed to have relaxations equal to the average of the Si atoms they are bridging, while terminal O5 and O6 relaxations are allowed to move independently from the Si_2 and Si_3 sites. The data are compared to the relaxations obtained by DFT calculation for an inner-sphere (IS) and outer-sphere (OS) Rb adsorbed onto the quartz(101) surface (green triangles and orange squares respectively). For DFT calculations, only one layer relaxation was explored.

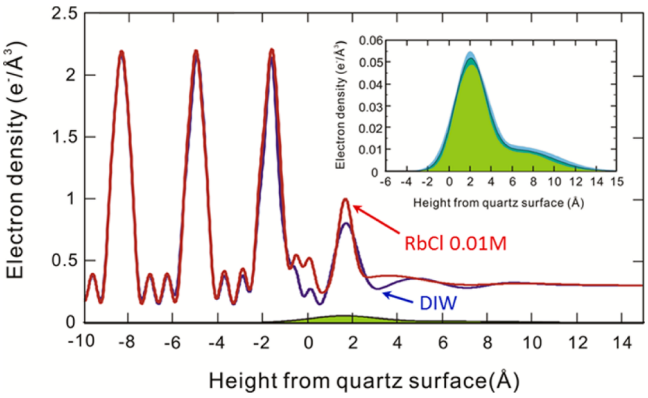

Figure 6. Derived electron density profiles for quartz(101) in contact with DIW (blue line) and 0.01 M RbCl solution at pH 9.8 (red line). The surface is defined as the average position of O5−O6 in the *unrelaxed* structure. The green area is the Rb-specific electron density profile from the RAXR data fit using the two layer model. Inset: Detailed view of the Rb-specific electron density profile derived from analysis of the RAXR data. The one sigma uncertainty bands of the Rb profile is shown as blue shading.

0.07 ± 0.01 Rb/A_{UC}, respectively. The total Rb occupancy from this model is 0.23 ± 0.03 Rb/A_{UC}.

While the Rb distribution is well-described with this two-layer model, we found that it also can be modeled as a diffuse profile (see details in the Supporting Information). This model provided a similar quality of fit as compared to the two-layer model, and the profiles obtained from the two models are visually similar. Therefore, the two models cannot be uniquely distinguished by the present XR/RAXR data alone. However, the derived decay length (5.9 ± 1.1 Å), obtained by a quantitative comparison of the RAXR data to the diffuse profile model (as defined by the diffuse model parameters, including the Rb ion coverage, o_{Rb}, the exponential decay length of the Rb distribution, λ_{Rb}, the height of the start of the exponential distribution, z_o, and an rms broadening term, u_{Rb}) is much shorter than expected based on the Gouy−Chapman theory (30 Å). This discrepancy suggests that the diffuse profile may not be a correct description of the ion distribution.

3.4. DFT Calculations. Various DFT-derived quartz−water−RbCl models simulated two conditions; a neutral quartz(101) surface at pH 7 (i.e., with added Cl^-; Figure SI3a−c, Supporting Information), and a negatively charged surface that was obtained by removing a H^+ from the model (pH 12, Figure SI3d−j). The calculated energies can be compared directly within the same group (i.e., a through c and d through h), but not between these two groups, due to differences in the composition of the two systems.

The calculations at pH 7, where Rb^+ interacts with two surficial SiOH groups or with water molecules, respectively, show that Rb^+ adsorbs as both inner-sphere (IS) and outer-sphere (OS) complexes (Figure SI3b and Table SI-2). The adsorption heights of these two species were 2.28 and 5.98 Å. These heights are similar to the heights (1.8 ± 0.1 and 6.4 ±

DOI: 10.1021/jp510139t
J. Phys. Chem. C XXXX, XXX, XXX−XXX

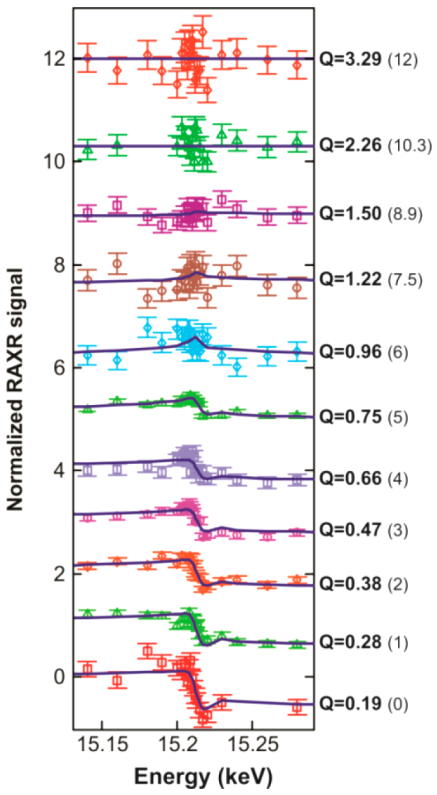

Figure 7. RAXR spectra collected near the Rb *K*-adsorption edge energy for quartz(101) in contact with 0.01 M RbCl at pH 9.8. The signal is normalized using the resonance amplitude normalization.[38] The scattering condition for each spectrum is defined by the momentum transfer *Q* (offset vertically by the number indicated in parentheses, for clarity).

1.0 Å, respectively) of the two Rb^+ species derived from the two-layer model for the RAXR data, albeit with some quantitative disagreements (Table 1). The calculated energy difference between these two states is −37 kJ/mol, indicating that IS Rb^+ is energetically more stable than OS Rb^+ at neutral pH. The surface − H_2O distances estimated from these models are 1.95 ± 0.1 and 4.82 ± 0.2 Å (Figure SI4); however, the potential systematic error on these values is large due to the fact that these estimates are derived from only a few configurations rather than thousands of configurations as would be the case from MD simulations. We also modeled the inner-sphere Rb^+ as an ion pair with Cl^-, and the energy was 2 kJ/mol lower than the Rb^+ ion inner-sphere model (Figure 8A). However, this is not a significant energy difference, and the calculation does not include entropic effects of forming the ion pair. The Rb^+ height was 2.34 Å in the RbCl ion pair model which is indistinguishable from the lone Rb^+ ion model.

The calculations for alkaline pH (pH = 12) were achieved by including negatively charged functional groups (SiO^-) at the surface, and the same models were subjected to energy minimization. Various combinations of IS Rb^+ configurations, such as Rb^+ bonded to two SiOH, one SiOH and one SiO^-, two SiO^- groups, and one SiO^-, as well as OS Rb^+ configurations (Figure SI3d−j) were examined. Three structures were found to have equivalent energetics: including IS Rb^+ bonded to one SiO^- surface group, OS Rb^+, and a fully solvated aqueous Rb^+ (Figure 8B−D and Table 2). Additionally, no DFT-derived structure reproduced the observed negative *z*-relaxations of the O5 and O6 atoms observed by XR (Table SI2).

4. DISCUSSION

4.1. Quartz(101)−Water Interface. Comparison with Previous Data. The main features of the derived interfacial structures and associated electron density profiles are generally consistent with previous work. Our results show agreement in the position of the first water layer (~1.9 Å above the surface). However, there are also small differences between the results. For example, the first water layer determined by Schlegel et

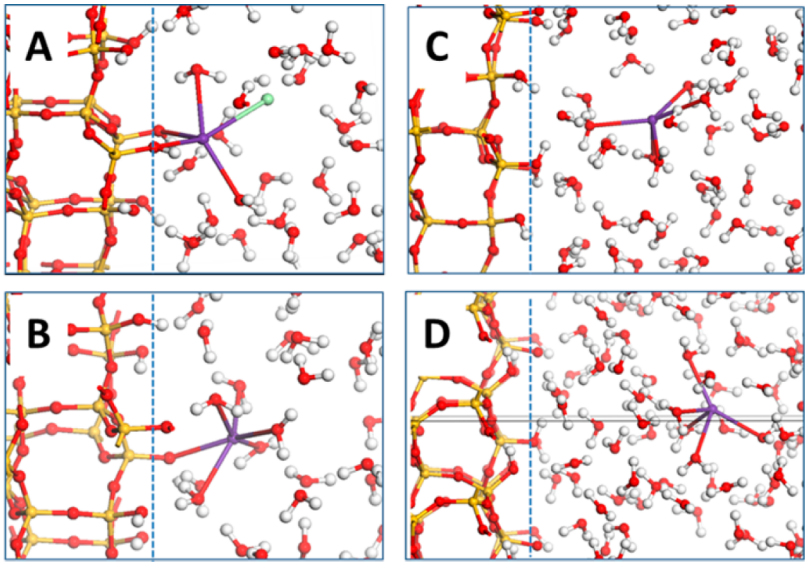

Figure 8. Final state of simulations based on DFT: yellow = Si; red = O; purple = Rb; green = Cl, white = H. The blue dashed line represents the reference point at the surface (corresponding to the average of O5 and O6 positions) from which Rb-surface distances are calculated. (A) Neutral surface with inner-sphere adsorption of a Rb−Cl ion pair (lowest nominal energy for the neutral surface models). Models in parts B−D show the negatively charged surface (pH 12), including: (B) inner-sphere Rb; (C) outer-sphere Rb; and (D) a fully solvated Rb ion. The black lines in (part D represent the boundaries of the periodic boundary cell. For details see Table 2 and Table SI2.

DOI: 10.1021/jp510139t
J. Phys. Chem. C XXXX, XXX, XXX−XXX

Table 2. Vertical Si and O Displacements and Rb Heights for the DFT Calculations in Figure 8[a]

	neutral surface	negatively charged surface		
model	A	B	C	D
Si1	0.03	0.10	0.10	0.15
Si2	0.09	0.13	0.15	0.18
Si3	0.19	0.25	0.25	0.37
O5	0.03	0.08	0.10	0.1
O6	0.16	0.24	0.24	0.36
Rb[b]	2.34	3.24	4.34	9.37 (aq)

[a]Displacements are reported as differences from the unrelaxed position of the specific atom in the *unrelaxed* bulk crystalline lattice. All values in Å. [b]Distance from the average position of O5/O6 in the *unrelaxed* bulk crystalline lattice.

al.[33] is broader than that in the current study. This difference may be related to difference in surface quality. In fact, the previous data, measured on annealed samples, had a roughness (3 Å rms variation, $\sigma_{rms} = d\beta^{1/2}/(1-\beta))$[29] that is twice as large as the present pretreated sample (1.5 Å). The present study also distinguishes an additional broader distribution of water at 4.8 Å from the surface, occurrence of which was not considered in the previous study. These derived water heights are in good agreement with those derived from the DFT calculations (1.95 ± 0.1 and 4.82 ± 0.2 Å, respectively).

The large and negative relaxation (i.e., toward the crystalline bulk) of the terminal oxygens observed in this study is consistent with that reported by Schlegel et al.,[33] with apparent shortening of the Si2−O5 and Si3−O6 vertical separations of −0.24 and −0.40 Å respectively. These shifts are too large to be justified by simple shortening of the Si−O bond distances, and therefore suggest that they may be due to tilting of the Si−O bond of the terminating oxygens (or hydroxyl groups). This feature seems to be unique to the quartz(101) surface, as similar studies on other oxides−solution interfaces reported positive displacements of the terminal oxygens, while negative relaxations larger than −0.1 Å have not been observed. For example, relaxations of terminal oxygens of Al_2O_3 (012) where reported to be +0.04 and −0.09 Å in DIW.[45] Large positive relaxations (+0.13 and +0.20 Å) were observed for the terminal oxygens at the TiO_2 (110) − DIW interface, whereas the magnitudes decreased to +0.06 and +0.03 Å in contact with 1 M pH12 RbCl solution.[46] These results suggest that the quartz surface relaxations have peculiar characteristics that might affect the mineral-solution interaction as well as the water and ion structuring at the interface.

Despite generally good agreement between XR/RAXR and DFT results, we find that there is a nontrivial discrepancy between the experimental and calculated results involving the interfacial displacements of the surface (hydroxyl) oxygens (specifically, O5 and O6). XR results indicate large *negative* displacements (−0.2 to −0.4 Å toward the bulk crystal), while DFT results indicate relatively smaller and *positive* displacements (+0.01 to +0.23 Å). We do not think that this is due to any fundamental limitations of the calculation, because the same general approach has been well-validated in previous studies on the TiO_2 (110) system.[35,47] To test whether this difference is due simply to the convergence of our structural model, we have refit the XR data by assuming the O5 and O6 positions as defined from the DFT calculations. While the quality of fit was worse, the heights of the interfacial water layers with respect to the DFT-derived average height of the O5 and O6 atoms remained unchanged (data not shown). Thus, while we do not understand the source of this discrepancy in O5 and O6 heights, it does not significantly alter the conclusions associated with the interfacial water and adsorbed ion structures.

The key to this peculiarity might reside in some fine detail of the surface structure that we have not yet constrained. First of all, the actual surface used in the experiments likely differs from the idealized surface used in the model calculations. The natural quartz surface has a finite roughness (as derived from the Robinson roughness factor) which results from the presence of numerous steps/kinks and pits at the surface. More directly, our best-fit models include Si atom vacancies (i.e., ∼10% in the top unit-cell layer) in the quartz surface. Qualitatively, these surface displacements are likely to have a role into accommodating water molecules and Rb^+ ions at the surface.

4.2. Rb Adsorption. Both the RAXR data and the DFT calculations suggest the presence of Rb adsorbed as discrete inner- and outer-sphere complexes.[48] The coexistence of multiple adsorbed species has been observed at the surfaces of silicates[38,49] and oxides[47] in contact with aqueous solutions. The Rb heights (1.8 ± 0.1 and 6.4 ± 1.0 Å above the average surface oxygen position) derived from the RAXR measured at pH 9.8 show good agreement with the heights of a stable IS species and a metastable OS species (∼2.3 and ∼6.0 Å, respectively) obtained from the DFT calculations at neutral pH. However, those heights do not match the heights of the most stable IS (monodentate) and OS species (∼3.2 and ∼4.3 Å, respectively; Figure 8) determined by DFT at more alkaline condition (pH 12). In particular, the height of the first layer from RAXR shows better agreement with the heights of binuclear-bidentate IS complexes (i.e., that bind to two surface functional groups), which are energetically less stable than the monodentate IS Rb^+ species. The quantitative differences between the RAXR and DFT results for the IS Rb species can be understood from observation (by RAXR) that this species has an inherently large distribution width (1.4 Å). This suggests that this species may involve multiple elementary adsorption configurations at the surface that might not be explored fully by the DFT results. While the RAXR and DFT results are not in full quantitative agreement with respect to this species, we consider the results to be qualitatively consistent.

The best-fit model for the Rb distribution nominally shows that a small portion (∼5%) of the Rb distribution at heights *below* the quartz surface (defined by the average surface oxygen height). To understand this, a few issues must be kept in mind. First, the origin is chosen as the *average* height of the surface oxygens. There may be space for the Rb ions between these functional groups, especially since the natural surfaces used in these measurements have an intrinsic roughness (1.5 Å) and a small Si vacancy concentration (∼10%) in the top unit-cell layer. Second, the derived Rb distribution has an inherent resolution of ∼1 Å (defined by the finite Q-range of the RAXR spectra), and therefore the extreme tail of the Rb distribution extending into the quartz surface is partially an artifact of the experimental resolution. Finally, the inherent Rb distribution for the IS species may be intrinsically asymmetric, but the model to which we fit the data used a symmetric Gaussian function. In this case, the current model may overestimate the width of the Rb distribution toward the quartz crystal although we expect that the coverage, average height and overall width (e.g., full width at half-maximum) will be robust.

DOI: 10.1021/jp510139t
J. Phys. Chem. C XXXX, XXX, XXX−XXX

We also compare the relative coverages of the IS and OS species with the energy differences calculated by DFT. The small calculated energy difference between the OS and IS Rb^+ species at pH 12 (6 kJ/mol; Table SI2) suggests that the two species should have similar coverages. This difference in calculated energy is also small with respect to the uncertainty in the calculation, as well as the energy of the fully hydrated Rb ion. This result is generally consistent with the RAXR results which show that both the IS and OS species are present, but with a coverage of IS Rb^+ that is larger than that of OS Rb^+. The inferred free energy difference between these two states from the RAXR-derived coverages, $\Delta G^\circ = -RT \ln(Occ_{OS}/Occ_{IS})$, is ~2.2 kJ/mol, comparable to the DFT calculation. Some differences between the XR/RAXR and DFT results are likely to arise from the differences in solution conditions in the measured and calculated systems (specifically the differences in pH).

4.3. Implications for Quartz(101) Surface Charge. The surface charge of SiO_2 polymorphs has been the subject of numerous studies.[10,11,15,16,50,51] SiO_2 polymorphs have negative surface charge in most aqueous conditions because of their low PZC. However, the absolute surface charge magnitude at a given pH is difficult to determine because it is generally calculated based on an assumed PZC which can vary in a wide range (from 2.1 to 3.8). Furthermore, titration studies are limited to the range of pH < 9.5 due to the increasing dissolution at more alkaline pH.

The Rb coverage measured by RAXR provides a new way to obtain experimental estimates of the quartz(101) surface charge. The experiments were conducted in a dilute solution (0.01 M) with a chemically simple Rb^+, indicating that the effects from other processes, such as the formation of ion pair[52,53] and the ion−ion correlation[54] are negligible. It is important to note, however, that the present results should reflect the adsorbed ion coverage within ~20 Å of the quartz surface, but that the presence of any classical diffuse ion profile with a decay length defined by the Gouy−Chapman theory would be effectively invisible to the present measurements. Consequently, we expect that our observations provide an approximate lower bound on the actual surface charge.

We use the two-layer Rb model as our benchmark for estimating the surface charge. The inferred surface charge of -0.11 ± 0.02 C/m^2 (0.23 ± 0.03 e^-/A_{UC}) shows good agreement with the range of the surface charge magnitudes reported in the literature under similar conditions.[10,11,15] For example, very good agreement exists between the present results and quartz powder titration experiments in 0.01 M NaCl[55,56] (Supporting Information). Additionally, our results are consistent with the surface charge of SiO_2 powder (−0.11 to −0.23 C/m^2) directly measured in alkali metal solutions at pH ~8.5.[15] Other studies have estimated the surface charge of quartz and silica based on their PZC; the surface charge of silica in 0.01N NaCl solution at pH 10 using an estimated PZC = 3.5 was -0.13 ± 0.01 C/m^2,[10] which is very similar to the present result. Another estimation of the surface charge of natural quartz using a PZC between 2 and 3[11] ranged from ~0.10 to 0.40 C/m^2 depending on the background electrolyte concentration (0.001 to 1 M KNO_3). While the surface charge reported for low ionic strength solutions is consistent with the present results, the estimation of the surface charge in 1 M KNO_3 apparently deviates from those measured from RAXR in our study, indicating that the difference in the ionic strength as well as the type of cations may be important controlling factors.

It is important to emphasize that the present measurements estimate the surface charge of a single crystallographically defined surface, while titration methods necessarily average over all surfaces. While our approach is not necessarily accurate (since we need to make assumptions to infer the surface charge), it has the advantage of being able to compare directly to theoretical and computational studies. Also, this approach can be used to estimate the surface charge at extreme pH (>10) where silica dissolves and therefore titration approaches cannot be used. Finally this approach opens up the possibility of probing the crystallographic anisotropy of surface charge, which can be used to extrapolate between well-defined model systems and the more complex and more widely studied mineral powders.

5. CONCLUSIONS

Specular X-ray reflectivity, resonant anomalous X-ray reflectivity and density functional theory were used to characterize the vertical structure of the natural quartz(101)−liquid interface, with quartz in contact with DIW and with RbCl solutions from neutral to alkaline conditions (pH from 7 to 12). Interfacial water structuring was observed at the interface, with two water layers at heights of 1.9 and 4.1−5.0 Å above the quartz surface. Rb adsorption was best described using a two-layer distribution (with Rb heights at 1.8 and 6.4 Å) corresponding to coexisting IS and OS species. The total Rb coverage estimated from this model is ~0.23 Rb atoms/A_{UC}, corresponding to a surface charge of −0.11 C/m^2, assuming that the surface charge is fully compensated by Rb^+ adsorption. DFT simulations of the quartz(101)−RbCl system are in good agreement with these results. The interfacial structural relaxations observed in the top three layers of the quartz surface (<0.1 Å for Si atoms and <0.4 Å for the terminal oxygens O5 and O6) obtained by XR were similar to and without Rb, and were in good agreement with previously published data.[33] However, the magnitude and direction of the O5 and O6 relaxation obtained by XR (i.e., large and negative) were inconsistent with those obtained from the DFT simulations (i.e., small and positive), suggesting that some aspect of the quartz−water interfacial structure remains unexplained. These results provide a direct test of the accuracy and robustness of our understanding of cation adsorption to quartz surfaces, and are a basis on which further studies on the effect of cation adsorption on the quartz dissolution process will be understood.

■ ASSOCIATED CONTENT

Ⓢ Supporting Information

Model-independent RAXR analysis, RAXR data fit using a diffuse ion-distribution model, DFT calculations, and quartz surface charge. This material is available free of charge via the Internet at http://pubs.acs.org.

■ AUTHOR INFORMATION

Corresponding Author

*(P.F.) Telephone: (630)252-7053. E-mail: fenter@anl.gov.

Notes

The authors declare no competing financial interest.

■ ACKNOWLEDGMENTS

This work was supported by the Division of Chemical Sciences, Geosciences and Biosciences, Office of Basic Energy Sciences, United States Department of Energy. The X-ray data were

DOI: 10.1021/jp510139t
J. Phys. Chem. C XXXX, XXX, XXX−XXX

collected at beamlines 6-ID-B and 33-ID-D, Advanced Photon Source. Use of the Advanced Photon Source was supported by the U.S. Department of Energy, Office of Science, Office of Basic Energy Sciences, under Contract DE-AC02-06CH11357 to UChicago Argonne, LLC as operator of Argonne National Laboratory.

REFERENCES

(1) Koretsky, C. M.; Sverjensky, D. A.; Sahai, N. A Model of Surface Site Types on Oxide and Silicate Minerals Based on Crystal Chemistry: Implications for Site Types and Densities, Multi-Site Adsorption, Surface Infrared Spectroscopy, and Dissolution Kinetics. *Am. J. Sci.* **1998**, *298*, 349−438.

(2) Brown, G. E., Jr.; Calas, G. Mineral-Aqueous Solution Interfaces and Their Impact on the Environment. *Geochem. Perspect.* **2012**, *1*, 483−742.

(3) Putnis, C. V.; Ruiz-Agudo, E. The Mineral-Water Interface: Where Minerals React with the Environment. *Elements* **2013**, *9*, 177−182.

(4) Szymczak, P.; Ladd, A. J. C. Wormhole Formation in Dissolving Fractures. *J. Geophys. Res.—Solid Earth* **2009**, *114*, B06203−1−22.

(5) Anovitz, L. M.; Cole, D. R.; Rother, G.; Allard, L. F.; Jackson, A. J.; Littrell, K. C. Diagenetic Changes in Macro- to Nano-Scale Porosity in the St. Peter Sandstone. An (Ultra) Small Angle Neutron Scattering and Backscattered Electron Imaging Analysis. *Geochim. Cosmochim. Acta* **2013**, *102*, 280−305.

(6) Nesbitt, H. W.; Young, G. M. Prediction of Some Weathering Trends of Plutonic and Volcanic Rocks Based on Thermodynamic and Kinetic Considerations. *Geochim. Cosmochim. Acta* **1984**, *48*, 1523−1534.

(7) Lasaga, A. C. Chemical-Kinetics of Water-Rock Interactions. *J. Geophys. Res.* **1984**, *89*, 4009−4025.

(8) Schulz, M. S.; White, A. F. Chemical Weathering in a Tropical Watershed, Luquillo Mountains, Puerto Rico III: Quartz Dissolution Rates. *Geochim. Cosmochim. Acta* **1999**, *63*, 337−350.

(9) Rimstidt, J. D. Quartz Solubility at Low Temperatures. *Geochim. Cosmochim. Acta* **1997**, *61*, 2553−2558.

(10) Bolt, G. H. Determination of the Charge Density of Silica Sols. *J. Phys. Chem.* **1957**, *61*, 1166−1169.

(11) Ahmed, S. M. Studies of the Dissociation of Oxide Surfaces at the Liquid−Solid Interface. *Can. J. Chem.* **1966**, *44*, 1663−1670.

(12) Kosmulski, M. Standard Enthalpies of Ion Adsorption onto Oxides from Aqueous-Solutions and Mixed-Solvents. *Colloid Surf. A* **1994**, *83*, 237−243.

(13) Kosmulski, M. Coadsorption of Monovalent and Multivalent Ions on Silica and Alumina. *Ber. Bunsen. Phys. Chem.* **1994**, *98*, 1062−1067.

(14) Kosmulski, M. The pH-Dependent Surface Charging and the Points of Zero Charge. *J. Colloid Interface Sci.* **2002**, *253*, 77−87.

(15) Dove, P. M.; Craven, C. M. Surface Charge Density on Silica in Alkali and Alkaline Earth Chloride Electrolyte Solutions. *Geochim. Cosmochim. Acta* **2005**, *69*, 4963−4970.

(16) Kosmulski, M. The pH-Dependent Surface Charging and Points of Zero Charge: V. Update. *J. Colloid Interface Sci.* **2011**, *353*, 1−15.

(17) Dove, P. M. The Dissolution Kinetics of Quartz in Aqueous Mixed Cation Solutions. *Geochim. Cosmochim. Acta* **1999**, *63*, 3715−3727.

(18) Gratz, A. J.; Bird, P. Quartz Dissolution - Negative Crystal Experiments and a Rate Law. *Geochim. Cosmochim. Acta* **1993**, *57*, 965−976.

(19) Gratz, A. J.; Bird, P.; Quiro, G. B. Dissolution of Quartz in Aqueous Basic Solution, 106−236°C - Surface Kinetics of "Perfect" Crystallographic Faces. *Geochim. Cosmochim. Acta* **1990**, *54*, 2911−2922.

(20) Brady, P. V.; Walther, J. V. Controls on Silicate Dissolution Rates in Neutral and Basic pH Solutions at 25°C. *Geochim. Cosmochim. Acta* **1989**, *53*, 2823−2830.

(21) Dove, P. M.; Crerar, D. A. Kinetics of Quartz Dissolution in Electrolyte-Solutions Using a Hydrothermal Mixed Flow Reactor. *Geochim. Cosmochim. Acta* **1990**, *54*, 955−969.

(22) Berger, G.; Cadore, E.; Schott, J.; Dove, P. M. Dissolution Rate of Quartz in Lead and Sodium Electrolyte-Solutions between 25°C and 300°C - Effect of the Nature of Surface Complexes and Reaction Affinity. *Geochim. Cosmochim. Acta* **1994**, *58*, 541−551.

(23) Dove, P. M.; Nix, C. J. The Influence of the Alkaline Earth Cations, Magnesium, Calcium, and Barium on the Dissolution Kinetics of Quartz. *Geochim. Cosmochim. Acta* **1997**, *61*, 3329−3340.

(24) Dove, P. M.; Han, N.; Wallace, A. F.; De Yoreo, J. J. Kinetics of Amorphous Silica Dissolution and the Paradox of the Silica Polymorphs. *Proc. Natl. Acad. Sci. U.S.A.* **2008**, *105*, 9903−9908.

(25) Nangia, S.; Garrison, B. J. Reaction Rates and Dissolution Mechanisms of Quartz as a Function of pH. *J. Phys. Chem. A* **2008**, *112*, 2027−2033.

(26) Gratz, A. J.; Bird, P. Quartz Dissolution - Theory of Rough and Smooth Surfaces. *Geochim. Cosmochim. Acta* **1993**, *57*, 977−989.

(27) Dove, P. M.; Han, N.; De Yoreo, J. J. Mechanisms of Classical Crystal Growth Theory Explain Quartz and Silicate Dissolution Behavior. *Proc. Natl. Acad. Sci. U.S.A.* **2005**, *102*, 15357−15362.

(28) Kubicki, J. D.; Solo, J. O.; Skelton, A. A.; Bandura, A. V. A New Hypothesis for the Dissolution Mechanism of Silicates. *J. Phys. Chem. C* **2012**, *116*, 17479−17491.

(29) Robinson, I. Crystal Truncation Rods and Surface Roughness. *Phys. Rev. B* **1986**, *33*, 3830−3836.

(30) Feidenhans'l, R. Surface-Structure Determination by X-Ray Diffraction. *Surf. Sci. Rep.* **1989**, *10*, 105−188.

(31) Fenter, P. *X-Ray Reflectivity as a Probe of Mineral-Fluid Interfaces: A User Guide. In Applications of Synchrotron Radiation in Low-Temperature Geochemistry and Environmental Science*; Geochemical Society and Mineralogical Society of America: Washington DC, 2002; Vol. *49*, pp 149−220.

(32) Park, C.; Fenter, P. A. Phasing of Resonant Anomalous X-Ray Reflectivity Spectra and Direct Fourier Synthesis of Element-Specific Partial Structures at Buried Interfaces. *J. Appl. Crystallogr.* **2007**, *40*, 290−301.

(33) Schlegel, M. L.; Nagy, K. L.; Fenter, P.; Sturchio, N. C. Structures of Quartz (10−10) and (10−11)-Water Interfaces Determined by X-Ray Reflectivity and Atomic Force Microscopy of Natural Growth Surfaces. *Geochim. Cosmochim. Acta* **2002**, *66*, 3037−3054.

(34) Skelton, A. A.; Fenter, P.; Kubicki, J. D.; Wesolowski, D. J.; Cummings, P. T. Simulations of the Quartz(10−11)/Water Interface: A Comparison of Classical Force Fields, Ab-Initio Molecular Dynamics and X-Ray Reflectivity Experiments. *J. Phys. Chem. C* **2010**, *115*, 2076−2088.

(35) Zhang, Z.; et al. Structure of Hydrated Zn^{2+} at the Rutile TiO_2 (110)-Aqueous Solution Interface: Comparison of X-Ray Standing Wave, X-Ray Absorption Spectroscopy, and Density Functional Theory Results. *Geochim. Cosmochim. Acta* **2006**, *70*, 4039−4056.

(36) Als-Nielsen, J.; McMorrow, D. *Elements of Modern X-Ray Physics*; Wiley: New York, 2011.

(37) Lee, S. S.; Park, C.; Fenter, P.; Sturchio, N. C.; Nagy, K. L. Competitive Adsorption of Strontium and Fulvic Acid at the Muscovite-Solution Interface Observed with Resonant Anomalous X-Ray Reflectivity. *Geochim. Cosmochim. Acta* **2010**, *74*, 1762−1776.

(38) Lee, S. S.; Fenter, P.; Park, C.; Sturchio, N. C.; Nagy, K. L. Hydrated Cation Speciation at the Muscovite (001)-Water Interface. *Langmuir* **2010**, *26*, 16647−16651.

(39) Bandura, A. V.; Kubicki, J. D.; Sofo, J. O. Periodic Density Functional Theory Study of Water Adsorption on the A-Quartz (101) Surface. *J. Phys. Chem. C* **2011**, *115*, 5756−5766.

(40) DelloStritto, M. J.; Kubicki, J.; Sofo, J. O. Density Functional Theory Simulation of Hydrogen-Bonding Structure and Vibrational Densities of States at the Quartz (101)-Water Interface and Its Relation to Dissolution as a Function of Solution pH and Ionic Strength. *J. Phys.: Condens. Matter* **2014**, *26*, 244101-1-11.

DOI: 10.1021/jp510139t
J. Phys. Chem. C XXXX, XXX, XXX−XXX

(41) Kresse, G.; Furthmuller, J. Efficient Iterative Schemes for Ab Initio Total-Energy Calculations Using a Plane-Wave Basis Set. *Phys. Rev. B* **1996**, *54*, 11169−11186.
(42) Perdew, J. P.; Burke, K.; Ernzerhof, M. Generalized Gradient Approximation Made Simple. *Phys. Rev. Lett.* **1996**, *77*, 3865−3868.
(43) Bandura, A. V.; Kubicki, J. D.; Sofo, J. O. Periodic Density Functional Theory Study of Water Adsorption on the Alpha-Quartz (101) Surface. *J. Phys. Chem. C* **2011**, *115*, 5756−5766.
(44) Kumar, N.; Kent, P. R. C.; Wesolowski, D. J.; Kubicki, J. D. Modeling Water Adsorption on Rutile (110) Using Van Der Waals Density Functional and DFT Plus U Methods. *J. Phys. Chem. C* **2013**, *117*, 23638−23644.
(45) Catalano, J. G.; Park, C.; Zhang, Z.; Fenter, P. Termination and Water Adsorption at the α-Al_2O_3 (012) - Aqueous Solution Interface. *Langmuir* **2006**, *22*, 4668−4673.
(46) Zhang, Z.; Fenter, P.; Sturchio, N. C.; Bedzyk, M. J.; Machesky, M. L.; Wesolowski, D. J. Structure of Rutile TiO_2 (110) in Water and 1 Molal Rb^+ at pH 12: Inter-Relationship among Surface Charge, Interfacial Hydration Structure, and Substrate Structural Displacements. *Surf. Sci.* **2007**, *601*, 1129−1143.
(47) Kohli, V.; Zhang, Z.; Park, C.; Fenter, P. Rb^+ and Sr^{2+} Adsorption at the TiO_2 (110)-Electrolyte Interface Observed with Resonant Anomalous X-Ray Reflectivity. *Langmuir* **2010**, *26*, 950−958.
(48) Stumm, W. *Chemistry of the Solid-Water Interface*; Wiley: New York, 1992.
(49) Fenter, P.; Park, C.; Sturchio, N. C. Adsorption of Rb^+ and Sr^{2+} at the Orthoclase (001)-Solution Interface. *Geochim. Cosmochim. Acta* **2008**, *72*, 1848−1863.
(50) Casey, W. H.; Lasaga, A. C.; Gibbs, G. V. Mechanisms of Silica Dissolution as Inferred from the Kinetic Isotope Effect. *Geochim. Cosmochim. Acta* **1990**, *54*, 3369−3378.
(51) Kosmulski, M. Compilation of PZC and IEP of Sparingly Soluble Metal Oxides and Hydroxides from Literature. *Adv. Colloid Interface Sci.* **2009**, *152*, 14−25.
(52) Penfold, R.; Nordholm, S.; Jonsson, B.; Woodward, C. E. A Simple Analysis of Ion-Ion Correlation in Polyelectrolyte Solutions. *J. Chem. Phys.* **1990**, *92*, 1915−1922.
(53) Barbosa, M. C. Ion-Ion Correlations in Charged Colloidal Suspensions. *Physica A* **2002**, *304*, 170−176.
(54) Martín-Molina, A.; Quesada-Pérez, M.; Galisteo-González, F.; Hidalgo-Álvarez, R. Looking into Overcharging in Model Colloids through Electrophoresis: Asymmetric Electrolytes. *J. Chem. Phys.* **2003**, *118*, 4183−4189.
(55) Riese, A. C. Ph.D. Thesis. Colorado School of Mines: Boulder, CO, 1982.
(56) Kosmulski, M.; Maczka, E.; Janusz, W.; Rosenholm, J. B. Multiinstrument Study of the Electrophoretic Mobility of Quartz. *J. Colloid Interface Sci.* **2002**, *250*, 99−103.

DOI: 10.1021/jp510139t
J. Phys. Chem. C XXXX, XXX, XXX−XXX